Bioorganic Chemistry 81 (2018) 356–361

Contents lists available at ScienceDirect

Bioorganic Chemistry

journal homepage: www.elsevier.com/locate/bioorg

Helix-loop-helix peptide foldamers and their use in the construction of hydrolase mimetics

Magda Drewniak[a,1], Ewelina Węglarz-Tomczak[a,1], Katarzyna Ożga[a], Ewa Rudzińska-Szostak[a], Katarzyna Macegoniuk[a], Jakub M. Tomczak[b], Magdalena Bejger[c], Wojciech Rypniewski[c], Łukasz Berlicki[a,*]

[a] Department of Bioorganic Chemistry, Wrocław University of Science and Technology, Wybrzeże Wyspiańskiego 27, 50-370 Wrocław, Poland
[b] Amsterdam Machine Learning Lab, University of Amsterdam, Science Park 904, 1098 XH Amsterdam, The Netherlands
[c] Institute of Bioorganic Chemistry, Polish Academy of Sciences, Noskowskiego 12/14, 61-704 Poznań, Poland

ARTICLE INFO

Keywords:
Foldamers
Peptides
Conformation
Circular dichroism
Nuclear magnetic resonance
Catalysis

ABSTRACT

De novo designed helix-loop-helix peptide foldamers containing *cis*-2-aminocyclopentanecarboxylic acid residues were evaluated for their conformational stability and possible use in enzyme mimetic development. The correlation between hydrogen bond network size and conformational stability was demonstrated through CD and NMR spectroscopies. Molecules incorporating a Cys/His/Glu triad exhibited enzyme-like hydrolytic activity.

1. Introduction

De novo construction of peptides with well-defined three-dimensional structures in solution is challenging. One of the possible approaches to this problem is the incorporation of unnatural amino acid residues in the peptide chain [1,2]. Peptide foldamers (i.e., molecules with a high propensity to form compact conformations) have been studied extensively for the last two decades [3–5]. For example, β-amino acid-containing peptides have been proven to show various folding patterns [6]. However, the vast majority of studied structures were composed of a single helix. Its geometry depended on the applied sequence pattern, structure and building block stereochemistry. One of the most interesting possibilities is the construction of α/β-peptides containing cycloalkane-based constrained β-amino acids [7]. 2-Aminocyclopentanecarboxylic acid (ACPC) stereoisomers are favourably used due to their feasible single enantiomer synthesis and straightforward incorporation into standard solid phase peptide synthesis (SPPS) protocols. αβ-Peptides containing *trans*-ACPC form 11- or 14/15-membered helices [8], while those containing *cis*-ACPC form 16/18-membered helices [9]. Peptides with other sequence patterns, including ααβ, αββ and ααββ, have also been studied [9–11]. However, more extended structures of foldameric peptides (i.e., containing more than one secondary element) are rarely reported. Recently, the Horne and Martinek groups (independently) have attempted to construct foldameric mini-proteins using a top-down approach where constrained fragments were incorporated in the known, well-folded α-peptidic structures [12,13].

Because peptide foldamers can be rationally designed, they are excellent scaffolds for construction of functional molecules [14]. Biologically active compounds [15], molecular sensors [16] and catalysts [17–19] have already been described. However, catalytic activity of β-amino acid-containing peptides have been shown in only limited number of examples including: hydrolase activity of β^3-peptide helix bundles, [18] aldolase activity of aggregating β-peptidic helices [17] and chorismate mutase activity of heterodimeric complex with β-amino acid containing fragments [19]. Aldol additions were also catalyzed by short, proline-containing peptide foldamers [20,21].

In this paper, we describe the *de novo* construction of a foldameric structure composed of two short helices connected by a flexible linker. We address the problem of controlling conformational stability by appropriately designing the hydrogen bond network. Subsequently, the elaborated helix-loop-helix scaffold is used for building esterase mimetics.

2. Results and discussion

To build helical fragments, the ααββ sequence pattern containing *cis*-ACPC residues of alternating stereochemistry were used [9]. Two

* Corresponding author.
E-mail address: lukasz.berlicki@pwr.edu.pl (Ł. Berlicki).
[1] M. D. and E. W.-T. contributed equally to this work.

https://doi.org/10.1016/j.bioorg.2018.07.012
Received 18 April 2018; Received in revised form 2 July 2018; Accepted 12 July 2018
Available online 17 July 2018

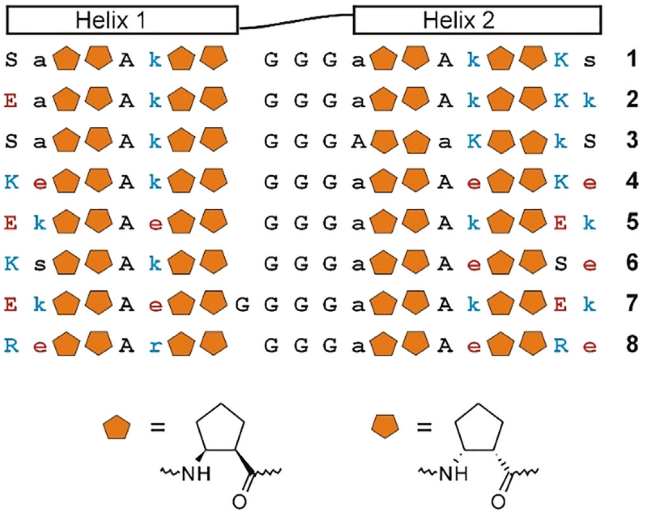

Fig. 1. Design principle and sequences of studied peptides. All peptides are N-acetylated and C-amidated. Positively and negatively charged residues are marked in blue and red, respectively. D- and L-amino acids are shown as small and capital letters, respectively.

short (8–9 residue) helical fragments were connected using an oligoglycine linker (Fig. 1). Solvent-exposed residues were designed to be hydrophilic (Lys/Glu/Ser/Arg), while the helical interface was built from *cis*-ACPC and alanine residues. Positively and negatively charged residues were placed in alternated way to form networks containing different numbers of inter- and intra-helical hydrogen bonds (Fig. S1). In addition, two peptides have a slightly modified scaffold: peptide **3** is composed of helices of opposite handedness, while peptide **7** has an elongated linker.

Peptides **1–8** were readily synthesized using a microwave-assisted solid phase approach. CD spectra revealed a high Cotton effect for most products (Fig. 2). The CD spectrum of the structure containing opposite-handed helices was close to zero, as contributions of both helices cancelled each other out.

Peptides **1** and **6** (dissolved in methanol) gave the lowest MRE values due to their minimal potential hydrogen bond network. Peptide conformational stabilities in aqueous solution (pH 7) were more diversified. The highest Cotton effect was observed for peptide **5**, where three pairs of Glu-Lys are present and both inter- and intra-helical interactions are possible. Interestingly, peptides containing reversed Glu/Lys residue positioning (structure **4**) or containing Arg-Glu pairs (peptide **8**) were less conformationaly stable. Moreover, the length of a linker between helices has significant impact in stability — peptide **7** with increased length by one Gly residue in comparison to peptide **5** has substantially decreased conformational stability. Thus, relative positioning of helices and possibility of appropriate inter-helical interactions are crucial for folding.

To confirm the influence of ion-pairing on conformational stability, pH dependences for peptide **1** and **5** were measured (Fig. S2). CD-monitored titration of peptide **1** showed a pK_a value of 9.33 ± 0.07, which is attributed to the deprotonation of lysine residues (Fig. S2A).

The high ellipticity increase observed at pH > pK_a indicates structure stabilization decrease of charge repulsion between lysine side chains upon deprotonation. In the case of peptide **5**, for which a dense hydrogen bond network is possible, the pattern is more complicated. The first pK_a value (4.92 ± 0.09) unambiguously describes deprotonation of glutamic acid side chains, while the second pK_a value (8.03 ± 0.22) was attributed to deprotonation of a lysine side chain (Fig. S2B). Deprotonation of both Glu residues and one of Lys residues enhanced peptide conformational stability, thus Glu-Lys and Lys-Lys interactions may occur.

Subsequently, we analysed the unfolding process of peptide **5** by monitoring the CD signal as a function of guanidine hydrochloride concentration and temperature (Fig. 3). Fitting experimental data to equations describing the thermodynamics of this process allowed us to find the thermodynamic parameters ($\Delta G^0 = 0.8 \pm 0.4$ kcal mol^{-1}, $\Delta H^0 = 3.6 \pm 0.4$ kcal mol^{-1}, $T\Delta S^0 = 2.8 \pm 0.4$ kcal mol^{-1}, $\Delta C_p = 0.00 \pm 0.01$ kcal mol^{-1} K^{-1} and $m = 0.24 \pm 0.06$ kcal mol^{-1} M^{-1}). Positive ΔG^0 values confirm that a fully folded helix-loop-helix structure prevails at room temperature. It is well-established that both ΔC_p and m values correlate well with the surface exposed to solvent upon unfolding [22]. Low values of these parameters indicate a small helical interface surface, which is expected for such short helices (two turns each). Therefore, the folding process is mainly driven by hydrogen bonds and electrostatic interactions (Lys/Glu), which is consistent with design principles.

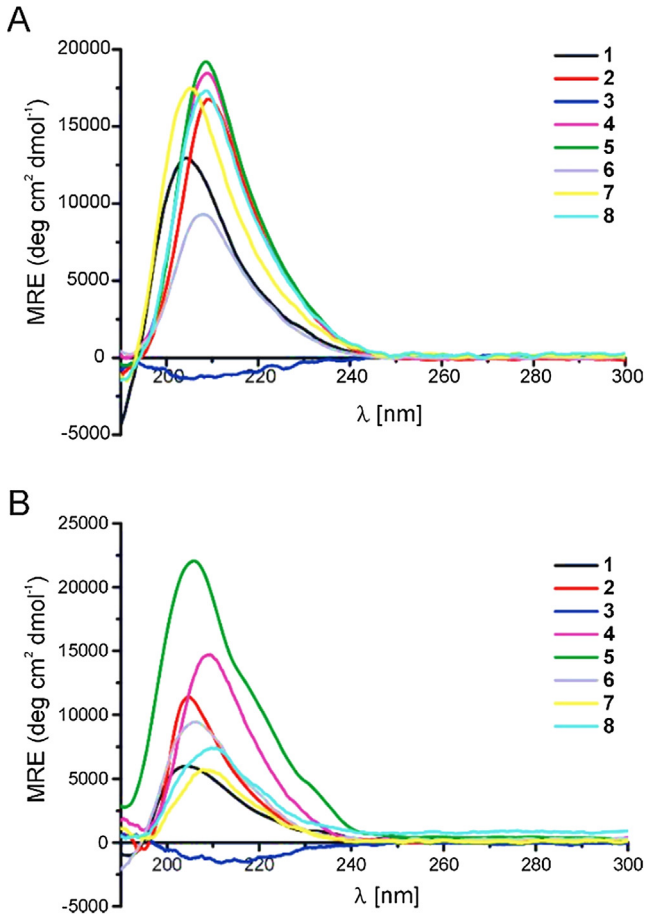

Fig. 2. Circular dichroism spectra of peptides **1–8** dissolved in methanol (A) and phosphate buffer pH 7 (B).

To confirm that the three-dimensional structure formation process of peptides **1–8** is driven exclusively by intramolecular interactions, dynamic light scattering analysis was performed (Figs. S3 and S4). In all studied cases, size distribution by mass clearly showed no aggregation and the hydrodynamic diameter (in a range of 1.58–2.22 nm) was consistent with models of folded peptides.

Subsequently, peptides **1–8** were studied using 2D NMR spectra (TOCSY and ROESY) to elucidate conformation in solution (Tables S2–S19). Careful analysis allowed assignment of all resonances in all peptides and detection of numerous non-sequential contacts. Contacts between residues i and $i-2$ or i and $i+2$ were consistent with the pattern observed previously for the 9/12/9/10-helical structure (Fig. S23) [9]. As expected, the oligo-glycine linker was not involved in helix formation and the above-mentioned non-sequential inter-proton interaction pattern was broken in this part of the sequence. Thus, the helix-loop-helix conformational arrangement was also reflected by the NMR-

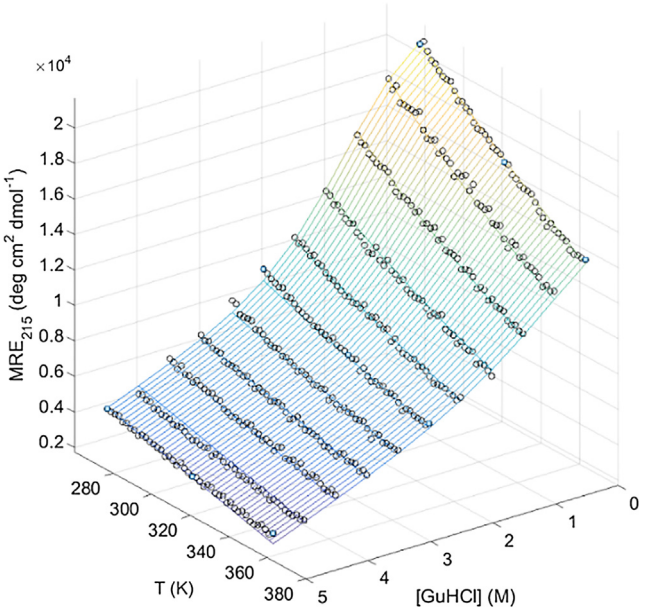

Fig. 3. Circular dichroism signature (Mean Residue Ellipticity at 215 nm, MRE_{215}) of peptide **5** unfolding as a function of temperature and guanidine hydrochloride concentration. Experimental data are shown as black circles, while fitted thermodynamic parameters for the folding equilibrium are represented by the surface.

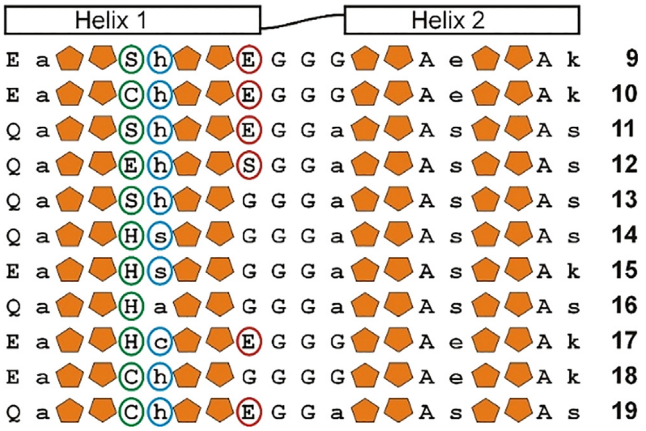

Fig. 4. Sequences of helix-loop-helix peptides with incorporated serine/cysteine hydrolase active site motifs. All peptides are N-acetylated and C-amidated. Orange pentagons denote *cis*-2-aminocyclopentane carboxylic acid residues, as in Fig. 1. Green, blue and red circles indicate residues designed to be catalytic.

derived inter-proton contact map. Using NMR restraints, the three-dimensional structure of peptide **5** was modelled and proven to be in the expected helix-loop-helix conformation (Fig. S24). Two well-ordered helices are joined by a poorly defined glycine linker. Moreover, unconstrained molecular dynamics simulations showed several possible interactions of Lys and Glu side chains, including both inter- and intra-helical interactions (Fig. S25). Although, relative positioning of two helices is not well-defined, it could be concluded that interactions between helices significantly increases their conformational stability.

Subsequently, we have used the helix-loop-helix scaffold for the construction of hydrolase mimetics. The Ser/His/Glu or Cys/His/Glu catalytic triads were incorporated to the *N*-terminal helix of the helix-loop-helix structure to obtain peptides **9** and **10**, respectively (Fig. 4 and Fig. S26). Interestingly, both peptides showed significant, but different, catalytic effects on hydrolysis of a model substrate (8-acetoxypyrene-1,3,6-trisulfonic acid trisodium salt, Table 1). Peptide **9** showed typical Michaelis-Menten kinetics with linear dependence of substrate formation on time, while progress curves of reactions catalysed by peptide **10** were biphasic (Fig. 5A). Several analogues of peptide **9**, compounds **11–16**, were obtained and analysed for their catalytic efficiency. Compound **11** lacked a Glu-Lys pair at termini, thus interactions between helices were weaker. Surprisingly, this change did not influence the k_{cat} value but decreased the K_m value, which could suggest that substrate binding is stronger and could occur between helices. Subsequently, changing active site residues by exchanging positions of Ser and Glu residues (peptide **12**), removing the Glu residue (peptides **13–15**) or removing both Ser and Glu residues (peptide **16**) did not influence kinetic parameters significantly. Thus, it could be concluded that histidine is the only catalytic residue in this system. Such effects on the hydrolytic activity of histidine-based catalysts have already been shown for other scaffolds [23,24,18].

Cysteine-based peptide catalysts (**10**, **17–19**) showed biphasic kinetics (Fig. S27–S28), which indicates the catalysed reaction has two steps involving acylation and hydrolysis of the acyl-peptide intermediate and the second step is rate limiting. Such behaviour has already been shown for both native enzymes (e.g., chymotrypsin) [25] and catalytic peptides incorporating the Cys/His/Glu triad [24]. An equation describing this type of kinetics ([product] = $B(1-e^{-bt}) + At$) [25] has been fitted to the progress curves (Fig. S29–S31), which allowed evaluation of the kinetic parameters of both steps (Fig. 5B and C). Importantly, all cysteine-based foldamers showed significantly higher k_{cat} values than other studied compounds and their catalytic efficiency is related to active site construction.

Reversal of the catalytic residue order (peptide **17**), removal of the Glu residue (peptide **18**) or removal of the terminal salt bridge (peptide **19**) caused decreased catalytic efficiency. In addition, the exchange of Cys residue by Ser (peptide **10** vs **9**) or by Ala (peptide **17** vs **16**) causes drop of activity and change of the shape of progress curves from biphasic to linear. Thus, Cys residue is crucial for the catalysis. While, comparison of peptide **16** containing only His as catalytic residue with peptide **4** (a negative control) confirms that His residue is an indispensable element of the catalytic system.

The described systems catalyse hydrolysis reactions by two different mechanisms, using either the histidine residue exclusively or the Cys-His-Glu triad. Both catalytic motifs have already been incorporated in various peptide-based scaffolds (Table S20) and exhibited similar efficiencies with observed k_2/K_s and k_{cat}/K_m values in the range of 0.1–405 $M^{-1} s^{-1}$ and 1.38–107 $M^{-1} s^{-1}$, respectively [18,23,24,26–30]. In particular, the described catalytic system is built in similar manner to that described by Woolfson [26]. Cys/His/Glu triad is placed on helical structure in both cases. Noteworthy, both systems have similar values of catalytic efficiency and analogous progress curves. However, the unique feature of the described foldamer-based catalytic system is its small molecular size. The high propensity of α/β-peptides to fold into well-defined structures allowed us to appropriately arrange catalytic residues in 20-mer peptides. The previously described catalysts were based on either much longer polypeptide chains or required oligomerization.

3. Conclusions

In summary, significant steps towards rational construction of foldamer-based protein-like structures were achieved. First, we have proven that small peptide foldamer conformational stability in aqueous solution could be effectively controlled by the formation of an appropriate hydrogen bond network. Second, non-aggregating peptide foldamers were shown to exhibit enzyme-like catalytic activity for the first time. Therefore, the construction of unprecedently small peptide-based artificial enzymes, which can be rationally designed and feasibly synthesized, proves the high potential of αβ-peptides in mimicking protein structures and functions.

Table 1
Kinetic parameters of peptides **9–19** in the hydrolysis of model substrate 8-acetoxypyrene-1,3,6-trisulfonic acid trisodium salt.

No.	Kinetics Type[a]	$k_2 \times 10^2$ (s^{-1})	K_s (μM)	k_2/K_s ($M^{-1} s^{-1}$)	$k_{cat} \times 10^4$ (s^{-1})[b]	K_m (μM)	k_{cat}/K_m ($M^{-1} s^{-1}$)
9	1	–	–	–	1.8 ± 0.2	4080 ± 890	0.044
10	2	3.5 ± 0.4	507 ± 22	69	26.4 ± 2.2	1360 ± 290	1.94
11	1	–	–	–	1.6 ± 0.3	467 ± 21	0.34
12	1	–	–	–	1.3 ± 0.4	378 ± 20	0.34
13	1	–	–	–	1.3 ± 0.4	382 ± 44	0.34
14	1	–	–	–	1.1 ± 0.3	490 ± 120	0.22
15	1	–	–	–	0.9 ± 0.3	545 ± 86	0.16
16	1	–	–	–	1.1 ± 0.5	372 ± 50	0.30
17	2	1.0 ± 0.1	222 ± 93	45	5.4 ± 0.6	2070 ± 320	0.26
18	1/2[c]	–	–	–	6.3 ± 1.6	687 ± 53	0.92
19	2	6.8 ± 2.1	2160 ± 180	3.2	5.3 ± 6.5	2000 ± 540	0.26

[a] Kinetics type 1 denotes linear dependence of product formation on time, while kinetics type 2 indicates biphasic progress curves.
[b] reaction is proceeding with $k = 5.6 \times 10^{-7} s^{-1}$ in presence of peptide **4** (a negative control).
[c] Although some progress curves are biphasic, the reliable calculation of k_2 and K_s values is not possible; thus a mixed mechanism was assumed.

4. Experimental

4.1. Peptide synthesis

All commercially available reagents and solvents were purchased from Sigma-Aldrich, Merck, Iris Biotech or Bachem and used without further purification. Both enantiomers of *cis*-cyclopentanocarboxylic acid (*cis*-ACPC) were obtained according to the literature [31] and the corresponding Fmoc-protected derivatives were synthesized from the amino-acid hydrochlorides according to the known procedure [32]. Peptide foldamers were obtained with an automated solid-phase peptide synthesizer (Biotage® Initiator + Alastra™) on H-Rink amide ChemMatrix® resin (loading: 0.59 mmol/g). Fmoc deprotection was achieved using 20% piperidine in DMF for 3 + 10 min. A double-coupling procedure was performed with 0.5 M solution of DIC and 0.5 M solution of OXYMA (1:1) in DMF, for α-amino acids 2 × 15 min, for β-amino acids 30 min, at 75 °C. Acetylation reaction was carried out using NMP/DIPEA/acetic anhydride (80:15:5) mixture. Cleavage of the peptides from the resin was accomplished with the mixture of TFA/TIS/H_2O (95:2.5:2.5) after 3 h of shaking. The crude peptide was precipitated with ice-cold diethyl ether and centrifuged (14 500 rpm, 2 × 5 min, 4 °C). Obtained peptide foldamers were purified using the HPLC (Knauer Prep) with a preparative column 250 mm × 30 mm, Thermo Scientific™ Hypersil GOLD™ (C18, 12 μm) and an analytical column 150 mm × 4.6 mm, Kinetex 100A (C18, 5 μm). Solvents and gradients are given below in results section (Table S1).

4.2. Mass spectrometry

Peptides were studied by WATERS LCT Premier XE System consisting of high resolution mass spectrometer with a time of flight (TOF).

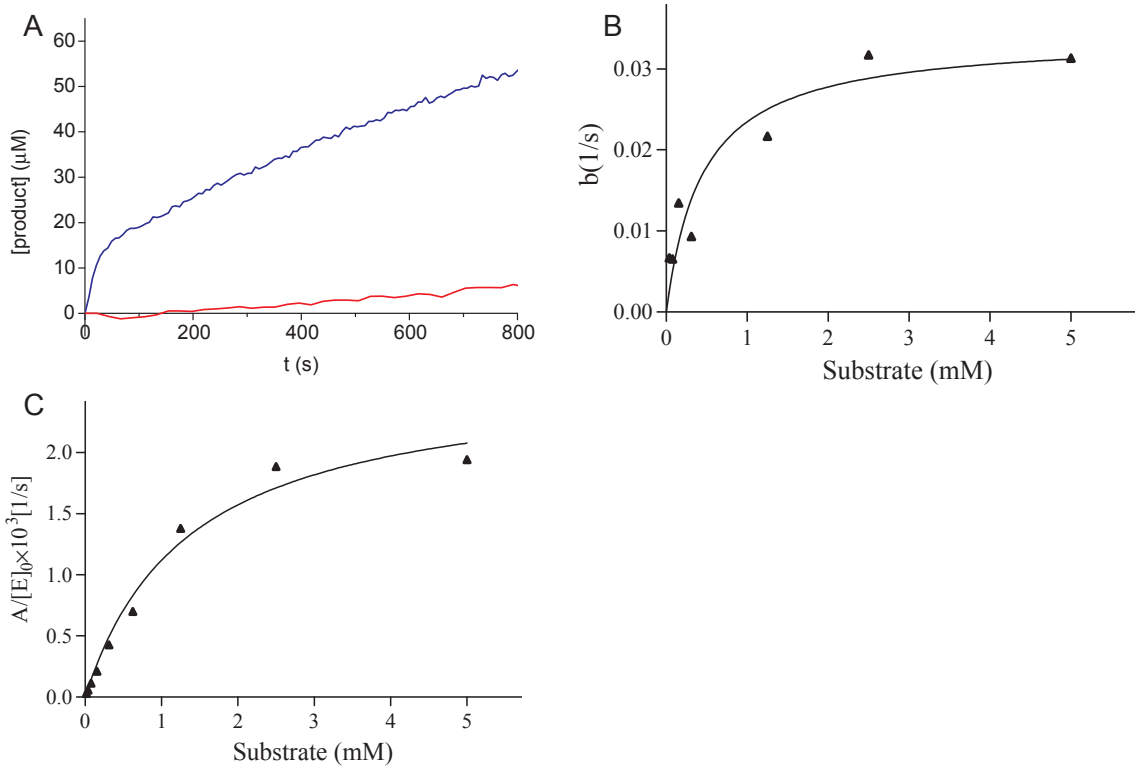

Fig. 5. Progress curves of 8-acetoxypyrene-1,3,6-trisulfonic acid trisodium salt (2.5 mM) hydrolysis catalyzed by peptide **10** (blue) and **9** (orange) (25 μM) (A), pre-steady-state analysis of the acylation events by the peptide **10**-catalyzed reaction (B) and a Michaelis–Menten plot for the turnover step of the peptide **10**-catalyzed reaction (C).

4.3. Circular dichroism

CD spectra were recorded on JASCO J-815 at 20 °C between 300 and 180 nm in methanol, and 50 mM Tris-HCl buffer (pH 7.0) using following parameters: 0.2 nm resolution, 1.0 nm band width, 20 mdeg sensitivity, 0.25 s response, 50 nm/min scanning speed, 3 scans, 0.02 cm cuvette path length. Typically, the sample was prepared using HPLC-purified and lyophilized peptide (as TFA salt) by dissolving 1.00 mg of peptide in 1.00 mL of methanol or buffer. The CD spectra of the solvents alone were recorded and subtracted from the raw data. The CD intensity is given as mean residue molar ellipticity (θ [deg × cm^2 × $dmol^{-1}$]).

4.4. pH titration

The stock solution of peptide was prepared by dissolving 2.00 mg of peptide in deionized water (2.00 mL). Initial pH was achieved upon addition of 10 mM HCl to stock solution. Subsequent addition of 2–10 µL aliquots of 10 mM NaOH allowed to obtain solutions of increasing pH. The samples of 60 µL volume were taken each time from stock solution to measure CD spectrum. The concentration of the peptide was adjusted for each spectrum on the basis of added volume of NaOH solution. pH were measured by S20 SevenEasy™ pH (Mettler Toledo). In order to evaluate pK_a values, equations given by Nielsen [33] were fitted to experimental data using Origin 9.0 software (OriginLab Corp.).

4.5. Temperature and [GuHCl]-dependent denaturation

To examine the thermal unfolding of the peptide, stock solutions were prepared containing 0.2 mg/mL peptide in 20 mM potassium phosphate buffer, pH 7.0, with 10 different concentrations of GuHCl. The temperature was increased from 4 to 90 °C in increments of 2 °C. Ellipticity measurements were recorded between 250 and 200 nm with 1 mm path length cuvette and 20 s averaging time, others parameters were unchanged.

4.6. Data modeling

Unfolding of peptides were monitored using CD spectra at 215 nm. Raw data were fitted to previously reported equations using nonlinear regression in Matlab R2016a (The MathWorks, Inc.). The observed elipticity (Q_{obs}) is dependent on equilibrium constant K and ellipticities of folded (Q_f) and unfolded states (Q_u):

$$Q_{obs} = \frac{1}{1+K}(Q_u * K + Q_f)$$

where Q_f and Q_u are dependent on both temperature and concentration of denaturant:

$$Q_u = a + bT + c[GuHCl]$$

$$Q_f = d + eT + f[GuHCl]$$

Equilibrium constant (K) is related to peptide folding free energy (ΔG):

$$K = e^{\frac{-\Delta G^0}{RT}}$$

While ΔG is given by formula:

$$\Delta G = \Delta H^0 - T\Delta S^0 + \Delta C_p\left(T - T_0 + T\ln\left(\frac{T_0}{T}\right)\right) - m[GuHCl]$$

4.7. NMR measurements

The NMR experiments were performed on Bruker Avance™ spectrometer operating at 600.58 MHz for ^{1}H, equipped with a 5.0 mm triple resonance probes: multi-nuclear broad-band observe probe or inverse probe for ^{1}H observe. TMS was used as the external standard. The NMR spectra at temperature ranging from 283 K to 298 K, as required for best spectral resolution, were recorded in a CD_3OH solution. The temperature was controlled to ± 0.1 K. Total correlation spectroscopy (TOCSY) and rotating frame Overhauser spectroscopy (ROESY) experiments were performed for chemical shift and structure assignment. All NMR spectra were acquired with presaturation of the solvent OH signal. Typical TOCSY - homonuclear Hartman-Hahn transfer using mlev17 sequence for mixing using two power levels for excitation and spinlock and 2D ROESY - with continuous wave spinlock for mixing were recorded in phase sensitive mode with the spectral width of 6127 Hz in both dimensions using 2048 data points and relaxation delay of 2 s. These spectra were acquired with 256 or 512 increments of 16 scans for TOCSY and 60–200 scans for 2D ROESY, depending on probe type and peptide concentration. TOCSY spectra were recorded with 60 ms mixing time. Spin lock time of the ROESY experiments was of 0.2 s. Processing and analysis of the NMR data were performed on Topspin 3.2 (Bruker BioSpin) software.

4.8. Dynamic light scattering

Peptides were tested for analyzer Zetasizer Nano (Malvern Instruments Ltd. 2013) to determine the hydrodynamic radius of particles in solution. Samples concentration were 10.0 mg/mL in water.

4.9. NMR structure calculation

The NMR structure generation and refinement was performed using Xplor-NIH v. 2.41 program [34]. NMR derived inter-proton contacts were classified by standard method with upper distance limits: strong 2.5 Å, medium 3.5 Å and weak 5 Å, and the lower distance limit was set to 1.8 Å. Initially, 50 random conformations of a peptide were generated. Restraints derived from ROE contacts and ^{3}J coupling constants of amide protons were included. Additionally, restraints for hydrogen bonding between residues 2 and 19 and between residues 6 and 16 were included. Standard protocols for NMR structure calculations implemented in Xplor-NIH were used. It is composed from the following steps: (1) high temperature dynamics (3500 K, 800 ps or 8000 steps), (2) simulated annealing performed from 3500 K to 25 K with 12.5 K step, at each temperature short dynamics was done (100 steps or 0.2 ps); (3) gradient minimization of final structure. Finally, top 10 lowest energy structures were superimposed.

4.10. Molecular dynamics

The molecular dynamics simulations were performed from folded NMR-derived starting structures using GROMACS v. 4.6.5 software suite [35] with the AMBER03 force field extended with cyclic beta-amino acids [36]. The simulations were carried out with explicit TIP3P solvent model in dodecahedron solvation boxes. The solvation of the peptides was done with the genbox utility available in GROMACS. Peptide 1 was neutralized by addition of three Cl^- ions in the system. Simulations were started from a previously minimized and equilibrated systems. For each peptide five independent production runs were carried out at 298 K for 10 ns with a step size of 2 fs. Neighbor searching was performed at every 10th step with a Verlet cut-off scheme. The particle mesh Ewald method was used for electrostatic interactions, with grid-spacing of 0.15 nm. The van der Waals interactions were computed from the neighborhood list with a cut-off of 1 nm. Temperature coupling was carried out with a V-rescale algorithm. Trajectories were analysed using Discovery Studio v. 4.1 software utilities.

4.11. Kinetic constants determination

Kinetic constants characterizing the hydrolysis of substrate

(substrate 8-acetoxypyrene-1,3,6-trisulfonic acid trisodium salt) in 50 mM Bis-Tris buffer, at pH = 6.0, peptide concentration 25–100 μM, substrate 0.0097–5 mM. Fluorogenic substrate: ATATS (acetoxypyrene-1,3,6-trisulfonic acid trisodium salt) is commercially available from Sigma Aldrich (Sigma Aldrich Poland, Poznań, Poland). Spectrofluorimetric measurements were performed on Spectra MAX Gemini EM fluorometer (Molecular Devices, Sunnyvale, USA). Kinetic measurements were performed in 96 well plate format working at two wavelengths: excitation at 460 nm and emission at 510 nm. Stock solution of peptide was prepared by dissolving 1.00 mg of peptide (purified using RP-HPLC and lyophilized) appropriate value of 50 mM bis-Tris buffer to achieve concentration of 1.0 mM. Peptides were pre-incubated for 30 min in a in 50 mM Bis-Tris buffer, at pH = 6.0. After incubation the peptides were added to the wells containing substrate. The release of the fluorophore was monitored continuously for at least 60 min at an peptides concentration of 25–100 μM and substrate 0.0097–5 mM (the total volume of 100 μL). In case of peptides that exhibit standard Michaelis Mentaen kinetic, the linear portion of the progress curve was used to calculate velocity of hydrolysis. Values of *K*m were calculated from the reaction velocity to substrate concentration plot using the Michaels-Menten equation ($V = V_{max} \times [S]/(K_m + [S])$ and $V_{max} = [E] \times k_{cat}$) with help of GraphPad Prism program (V – velocity of hydrolysis, V_{max} – maximum enzyme velocity, K_m – the Michaelis-Menten constant, $[S]$ – substrate concentration, k_{cat} – turnover number, $[E]$ – peptide concentration). In case of peptide that exhibit chymotrypsin-like mechanism fitting of the obtained curves from experiments was carried out following the method described by Bender et al. [23] and used recently by Burton et al. [24]. The progress curves were fitted to an equation with an exponential and a linear term ($y = B \times (1 - e^{-bx}) + Ax$, where y is product concentration and x is time) using SciPy package in Python version 2.7. Values of k_2, K_S, k_{cat} and K_m were calculated from the [E] and a/[E] to substrate concentration plot using the equations: ($b = k_2 \times [S]/(K_s + [S])$ and $A/[E] = k_{cat} \times [S]/(K_m + [S])$ with help of GraphPad Prism program (k_2 is the rate constant for acylation, K_s is the pseudo K_m for the acylation step[1]). The experiments were repeated at least three times and the average as well as the standard deviation values was calculated. The concentration of DMSO in the assay was less than 1% (v/v).

Acknowledgement

The work was financed by the National Science Centre, Poland (Grant No. DEC-2013/10/E/ST5/00625).

Appendix A. Supplementary material

Supplementary data associated with this article can be found, in the online version, at https://doi.org/10.1016/j.bioorg.2018.07.012.

References

[1] R.P. Cheng, S.H. Gellman, W.F. DeGrado, β-Peptides: from structure to function, Chem. Rev. 101 (2001) 3219–3232.
[2] W.S. Horne, S.H. Gellman, Foldamers with heterogeneous backbones, Acc. Chem. Res. 41 (2008) 1399–1408.
[3] S.H. Gellman, Foldamers: a Manifesto, Acc. Chem. Res. 31 (1998) 173–180.
[4] D. Seebach, J.L. Matthews, β-Peptides: a surprise at every turn, Chem. Commun. (1997) 2015–2022.
[5] T.A. Martinek, F. Fülöp, Peptidic foldamers: ramping up diversity, Chem. Soc. Rev. 41 (2012) 687–702.
[6] L.K. Pilsl, O. Reiser, α/β-Peptide foldamers: state of the art, Amino Acids 41 (2011) 709–718.
[7] F. Fülöp, T.A. Martinek, G.K. Tóth, Application of alicyclic beta-amino acids in peptide chemistry, Chem. Soc. Rev. 35 (2006) 323–334.
[8] S.H. Choi, I.A. Guzei, L.C. Spencer, S.H. Gellman, Crystallographic characterization of helical secondary structures in α/β-Peptides with 1:1 residue alternation, J. Am. Chem. Soc. 130 (2008) 6544–6570.
[9] Ł. Berlicki, L. Pilsl, E. Wéber, I.M. Mándity, C. Cabrele, T.A. Martinek, F. Fülöp, O. Reiser, Unique α, β- and α, α, β, β-peptide foldamers based on cis-β-aminocyclopentanecarboxylic acid, Angew. Chem. Int. Ed. 51 (2012) 2208–2212.
[10] S.H. Choi, I.A. Guzei, L.C. Spencer, S.H. Gellman, Crystallographic characterization of helical secondary structures in 2:1 and 1:2 α/β-peptides, J. Am. Chem. Soc. 131 (2009) 2917–2924.
[11] M. Szefczyk, E. Węglarz-Tomczak, P. Fortuna, A. Krzysztoń, E. Rudzińska-Szostak, Ł. Berlicki, Controlling the helix handedness of ααβ-Peptide foldamers through sequence shifting, Angew. Chem. Int. Ed. 56 (2017) 2087–2091.
[12] G. Olajos, A. Hetényi, E. Wéber, L.J. Németh, Z. Szakonyi, F. Fülöp, T.A. Martinek, Induced folding of protein-sized foldameric β-sandwich models with core β-amino acid residues, Chem. Eur. J. 21 (2015) 6173–6180.
[13] Z.E. Reinert, G.A. Lengyel, W.S. Horne, Protein-like tertiary folding behavior from heterogeneous backbones, J. Am. Chem. Soc. 135 (2013) 12528–12531.
[14] C.M. Goodman, S. Choi, S. Shandler, W.F. DeGrado, Foldamers as versatile frameworks for the design and evolution of function, Nat. Chem. Biol. 3 (2007) 252–262.
[15] C. Cabrele, T.A. Martinek, O. Reiser, Ł. Berlicki, Peptides containing beta-amino acid patterns—challenges and successes in medicinal chemistry, J. Med. Chem. 57 (2014) 9718–9739.
[16] B.A.F. Le Bailly, J. Clayden, Dynamic foldamer chemistry, Chem. Comm. 52 (2016) 4852–4863.
[17] M.M. Muller, M.A. Windsor, W.C. Pomerantz, S.H. Gellman, D. Hilvert, A rationally designed aldolase foldamer, Angew. Chem. Int. Ed. 48 (2009) 922–925.
[18] P.S.P. Wang, J.B. Nguyen, A. Schepartz, Design and high-resolution structure of a β3-peptide bundle catalyst, J. Am. Chem. Soc. 136 (2014) 6810–6813.
[19] C. Mayer, M.M. Müller, S.H. Gellman, D. Hilvert, Building proficient enzymes with foldamer prostheses, Angew. Chem. Int. Ed. 53 (2014) 6978–6981.
[20] O. Illa, O. Porcar-Tost, C. Robledillo, C. Elvira, P. Nolis, O. Reiser, V. Branchadell, R.M. Ortuño, Stereoselectivity of proline/cyclobutane amino acid-containing peptide organocatalysts for asymmetric aldol additions: a rationale, J. Org. Chem. 83 (2018) 350–363.
[21] V. D'Elia, H. Zwicknagl, O. Reiser, Short α/β-peptides as catalysts for intra- and intermolecular aldol reactions, J. Org. Chem. 73 (2008) 3262–3265.
[22] J.K. Myers, C.N. Pace, J.M. Scholtz, Denaturant m values and heat capacity changes: relation to changes in accessible surface areas of protein unfolding, Protein Sci. 4 (1995) 2138–2148.
[23] Y.S. Moroz, T.T. Dunston, O.V. Makhlynets, O.V. Moroz, Y. Wu, J.H. Yoon, A.B. Olsen, J.M. McLaughlin, K.L. Mack, P.M. Gosavi, N.A. van Nuland, I.V. Korendovych, New tricks for old proteins: single mutations in a nonenzymatic protein give rise to various enzymatic activities, J. Am. Chem. Soc. 137 (2015) 14905–14911.
[24] C.M. Rufo, Y.S. Moroz, O.V. Moroz, J. Stöhr, T.A. Smith, X. Hu, W.F. DeGrado, I.V. Korendovych, Short peptides self-assemble to produce catalytic amyloids, Nat. Chem. 6 (2014) 303–309.
[25] M.L. Bender, F.J. Kezdy, F.C. Wedler, alpha-Chymotrypsin: enzyme concentration and kinetics, J. Chem. Edu. 44 (1967) 84–88.
[26] J. Burton, A.R. Thomson, W.M. Dawson, R.L. Brady, D.N. Woolfson, Installing hydrolytic activity into a completely de novo protein framework, Nat. Chem. 8 (2016) 837–844.
[27] K.S. Broo, L. Brive, P. Ahlberg, L. Baltzer, Catalysis of hydrolysis and transesterification reactions of p-nitrophenyl esters by a designed helix − loop − helix dimer, J. Am. Chem. Soc. 119 (1997) 11362–11372.
[28] M.L. Zastrow, A.F.A. Peacock, J.A. Stuckey, V.L. Pecoraro, Hydrolytic catalysis and structural stabilization in a designed metalloprotein, Nat. Chem. 4 (2012) 118–123.
[29] B.S. Der, D.R. Edwards, B. Kuhlman, Catalysis by a de novo zinc-mediated protein interface: implications for natural enzyme evolution and rational enzyme engineering, Biochemistry 51 (2012) 3933–3940.
[30] D.N. Bolon, S.L. Mayo, Enzyme-like proteins by computational design, Proc. Natl. Acad. Sci. USA 98 (2001) 14274–14279.
[31] S.G. Davies, O. Ichihara, I. Lenoir, I.A.S. Walters, Asymmetric synthesis of (–)-(1R,2S)-cispentacin and related cis- and trans-2-amino cyclopentane- and cyclohexane-1-carboxylic acids, J. Chem. Soc. Perkin 1 (1994) 1411–1415.
[32] L. Lapatsanis, G. Milias, K. Froussios, M. Kolovos, Synthesis of N-2,2,2-(Trichloroethoxycarbonyl)-L-amino acids and N-(9-fluorenylmethoxycarbonyl)-L-amino acids involving succinimidoxy anion as a leaving group in amino acid protection, Synthesis (1983) 671–673.
[33] D. Farrell, E.S. Miranda, H. Webb, N. Georgi, P.B. Crowley, L.P. McIntosh, J.E. Nielsen, Titration_DB: storage and analysis of NMR-monitored protein pH titration curves, Proteins 78 (2010) 843–857.
[34] C.D. Schwieters, J.J. Kuszewski, G.M. Clore, Using Xplor-NIH for NMR molecular structure determination, Progr. NMR Spectrosc. 48 (2006) 47–62.
[35] H.J.C. Berendsen, D. van der Spoel, R. van Drunen, GROMACS: a message-passing parallel molecular dynamics implementation, Comp. Phys. Comm. 91 (1995) 43–56.
[36] L.J. Németh, Z. Hegedüs, T.A. Martinek, Predicting order and disorder for β-peptide foldamers in water, J. Chem. Inf. Mod. 64 (2014) 2776–2783.